Journal of Industrial and Engineering Chemistry 78 (2019) 232–238

Contents lists available at ScienceDirect

Journal of Industrial and Engineering Chemistry

journal homepage: www.elsevier.com/locate/jiec

Towards high performance of supercapacitor: New approach to design 3 D architectured electrodes with bacteria

Kwang Se Lee[a,b], Sang Jun Kim[a], Chan Woo Park[c], Incheol Cho[d], Patrick Joo Hyun Kim[b], Vilas G. Pol[b], Inkyu Park[d], Jang Myoun Ko[a,*]

[a] Department of Applied Chemistry & Biotechnology, Hanbat National University, San 16-1 Dukmyung-Dong, Yusung-Gu, Daejeon, 305-719, Republic of Korea
[b] Davidson School of Chemical Engineering, Purdue University, West Lafayette, 47907, USA
[c] Decontamination & Decommissioning Research Division, Korea Atomic Energy Research Institute, Daedeok-daero 989-111, Yuseong-gu, Daejeon, Republic of Korea
[d] Department of Mechanical Engineering, Korea Advanced Institute of Science and Technology (KAIST), 291 Daehak-ro, Yuseong-gu, Daejeon, 34141, Republic of Korea

ARTICLE INFO

Article history:
Received 9 April 2019
Received in revised form 5 June 2019
Accepted 6 June 2019
Available online 13 June 2019

Keywords:
Sponge
Bacteria
Zinc oxide
Supercapacitor
Electrode

ABSTRACT

A novel approach of preparing high performance electrodes for supercapacitors was demonstrated by pyrolyzing the hierarchical composite prepared from organic waste and biological resources. Sponge waste was utilized as a carbon source for preparing the interconnected structured electrode materials with high porosity, and needle-like ZnO particles were directly grown on the sponge in order to effectively capture bacteria cells as well as improve the overall redox reactions. The bacteria (*E. coli* O157: H7) were isolated on a ZnO/sponge composite to endow electrochemically beneficial inherent nitrogen existing in bacteria, as well as to provide bio-templates with the aids of these structural and material benefits, the carbonized material prepared from the bacteria loaded on the ZnO/sponge composite showed a significantly enhanced specific capacitance of 133 F g^{-1} (at 0.2 A g^{-1}) and an excellent cycle retention of 89% over long-term cycles (5000 cycles). Our strategy of utilizing recyclable and biomass-derived materials not only can effectively improve the electrochemical performances of supercapacitors but also open an innovative way to address the systemic issues underlying the carbonaceous materials used in supercapacitors.

Introduction

The sustainable chemistry for synthesizing functional new materials has received growing attention due to current environmental issues and limited resources [1,2]. Carbonized organic resources have been widely investigated for electrochemical application due to their high electrical conductivities. However, it was difficult to obtain a porous structure by itself without further treatment. The porous structures with a high surface area and contents of heteroatoms are essentially required for achieving high performance supercapacitors. The well-controlled porous structures from natural resources is still challenging, and template-based synthesis or harsh carbonization processes are generally required. Although renewable resources have been proposed previously for electrode materials, activation process using KOH [3,4], $ZnCl_2$ [5,6], and H_3PO_4 [7,8] are still required to produce porous structure.

The commercial sponges consisting of polyurethane are used as a cleaning tool for washing impervious surfaces and insulator including refrigerator, vehicle, and clothes. As the use of sponge enormously increases, the amount of sponge waste also keeps increasing every year. Previous investigation revealed that 7.5 million tons of polyurethane sponge were consumed in 2000's and their disposal rate is increasing [9]. A representative feature of sponge is that it intrinsically possesses hierarchical porous structures containing macro- and micro-pores, which does not require a further activation process to produce pores on the carbon scaffold. We assumed that the upcycling of disposable sponge into sustainable carbon material can be an innovative strategy to design the unique, hierarchical and porous-structured carbon for supercapacitors. In addition, the use of sponges as electrodes materials has not yet been reported to the best of our knowledge.

Bacteria is another natural resource that contains various heteroatoms including nitrogen which is a beneficial element for

* Corresponding author.
E-mail address: jmko@hanbat.ac.kr (J.M. Ko).

https://doi.org/10.1016/j.jiec.2019.06.010
1226-086X/

electrochemical properties of supercapacitor electrodes. Bacteria comprise a large domain of prokaryotic microorganisms with sturdy cell walls that maintain the whole cell system in harsh conditions [10,11]. In addition, they are inexpensive, abundant, environmentally benign, and renewable resources provided by nature. For these reasons, bacteria have become promising additives to produce electrode materials through nitrogen doping and enhancing electrical conductivity by delocalization of electrons. Bacteria have been used to prepare composite electrodes with transition metal oxide because the electrode materials exhibit pseudocapacitive behavior by redox reaction on interfaces between electrode and electrolyte [12–16]. Most recently, Atalay et al. reported the metal oxide nanostructures with high surface-to-volume ratio using the *Deinococcus radiodurans* bacteria [17]. This group developed a bio fabrication method with obtaining porous nanostructured nickel oxide for electrode material. Shim et al. demonstrated the preparation of porous Co_3O_4 nanostructures linked with *Bacillus subtilis* for lithium storage [18]. Previous studies revealed that bacteria provide superior properties for electrode materials with novel features.

Even though zinc oxide (ZnO) is considered as one of the most attractive electrode materials for supercapacitors owing to its high energy density (~760 A g^{-1}), environmental friendliness and cost-benefit, less effort has been devoted to designing carbon/ZnO composites [19]. An appropriate amount of ZnO can enhance the electrochemical performance due to function as efficient electron conducting pathway, indicating that the best electrochemical performances of ZnO composites can be achieved through adjusting the concentration of ZnO. Therefore, designing and developing the new framework of electrode material is necessary for enhancing the electrochemical properties.

In this paper, an efficient and straightforward approach to create hierarchical structured ZnO/carbon electrode for supercapacitors was demonstrated. First, intrinsically porous structure of sponge materials was employed to prepare porous carbon template via carbonization, which has not been reported yet. Second, needle-like ZnO nanoparticles were grown on the sponge in order to further capture bacteria and enhance the overall redox reactions. Third, the bacteria were isolated on ZnO/

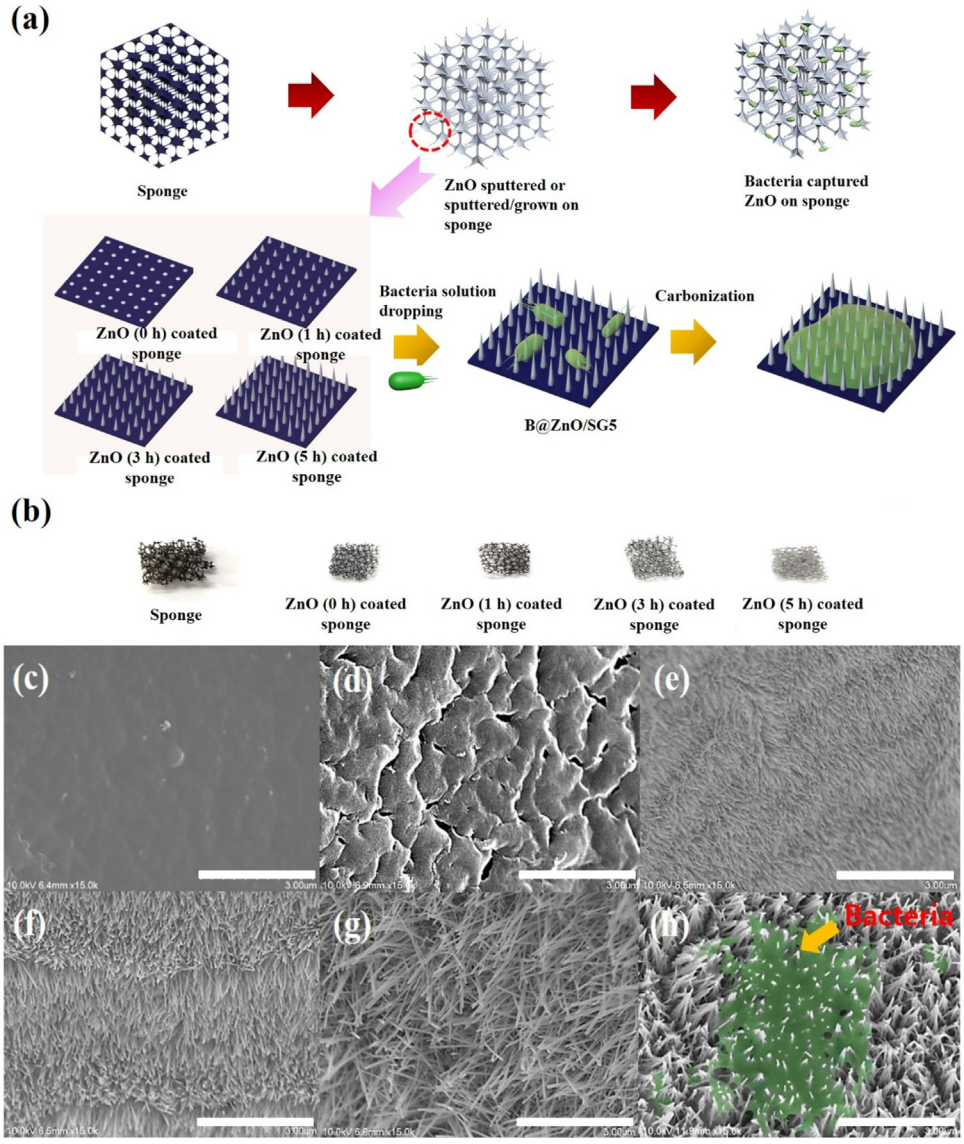

Fig. 1. (a) Schematic procedure of bacteria captured ZnO on sponge for electrode materials and (b) images of real samples of sponge and ZnO coated sponge with different growth time. FESEM images of (c) sponge, (d) ZnO (0 h) coated sponge, (e) ZnO (1 h) coated sponge, (f) ZnO (3 h) coated sponge, (g) ZnO (5 h) coated sponge, and (h) representative image of bacteria captured ZnO (5 h) coated sponge before carbonization (All scale bars are 3 μm).

sponge composites to endow intrinsic nitrogen in bacteria as well as to provide bio-template consisting of an outer membrane containing lipopolysaccharides, a periplasmic space with a peptidoglycan layer. To investigate how the ratio of ZnO nanowire to the entire electrode affect the electrochemical performances of supercapacitors, the length of ZnO nanowire was controlled. With the synergistic contribution of ZnO nanowire, bacteria derived carbon and sponge derived carbon, the prepared electrode exhibited an excellent capacitance and stable cyclability over 5000 cycles.

Experimental

Preparation of bacteria

E.coli O157:H7 (ATCC) cells were prepared in a 15 mL tube containing Luria Bertani (LB) broth (LPS solution Inc. Korea) and incubated overnight with shaking (150 rpm) at 37 °C. The cell density of bacteria was measured by UV absorption at 600 nm and the optical density was 1 which was equivalent to 10^9 cells/mL.

Preparation of sponge-based active materials for electrodes

First, a layer of ZnO was deposited on a sliced sponge by radio frequency (RF) sputtering (150 W, 10 min for both sides) as seeds of nanowires. Then, sponges were immersed in ZnO precursor solution (25 mM zinc nitrate hexahydrate containing 25 mM hexamethylenetetramine (HMTA) and 6 mM polyethyleneimine (PEI)) in DI water and heated at 95 °C for 0, 1, 3 and 5 h for the growth of ZnO [20]. Finally, the sponge was rinsed with DI water, followed by drying by nitrogen blowing. The pristine sponge (SG), bacteria doped ZnO/SG series (B@ZnO/SG) with different growth time (denoted B@ZnO/SG0, B@ZnO/SG1, B@ZnO/SG3, B@ZnO/SG5) were carbonized at 700 °C for 2 h under nitrogen atmosphere. (In case of bacteria doped samples, bacteria (1 mL) were dropped on the ZnO/sponge samples by pipette before carbonization).

Material characterization

The surface morphologies of prepared samples were measured using the Hitachi S-4800 field emission scanning electron microscopy (FESEM). Chemical compositions of the samples were

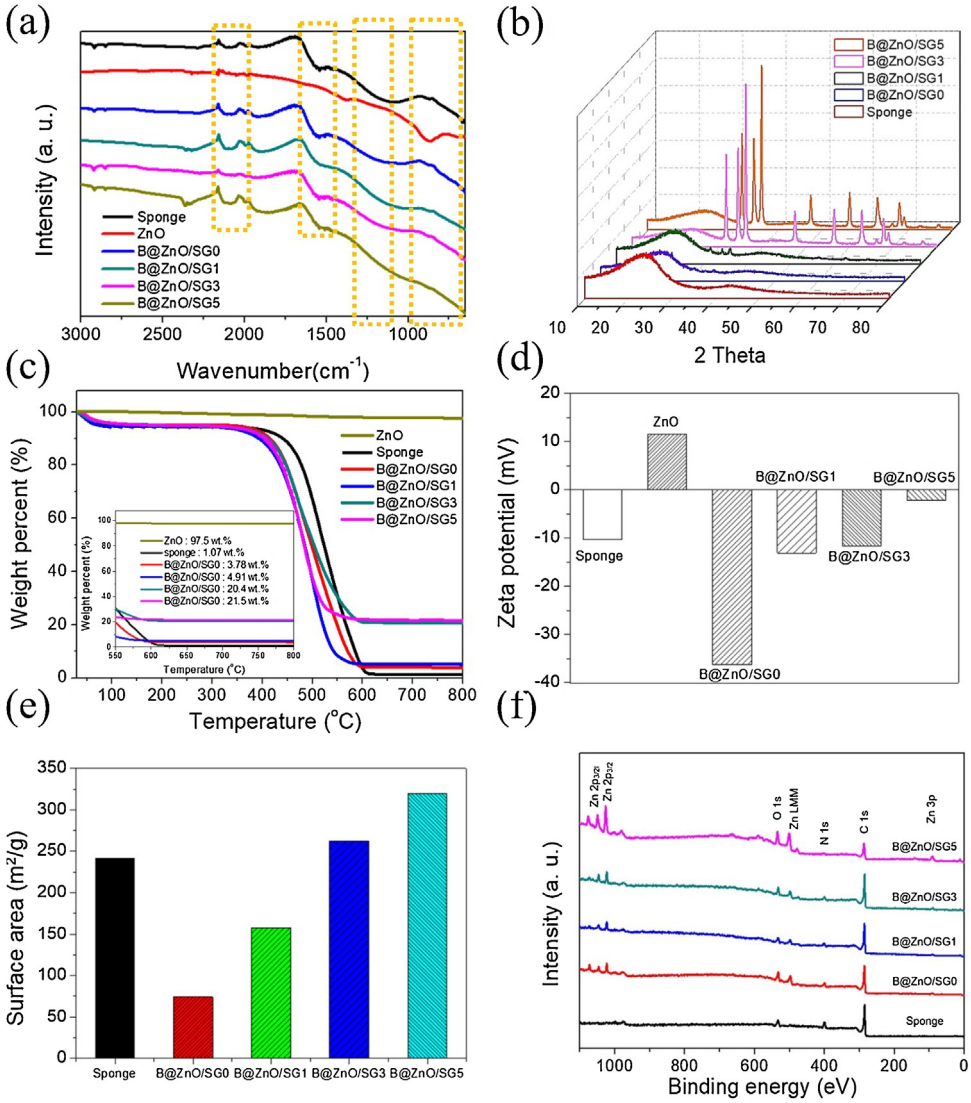

Fig. 2. (a) FTIR spectrum, (b) XRD patterns, (c) TGA results, and (d) zeta potentials, (e) BET analysis results, and (f) XPS surveys of sponge and bacteria captured ZnO on sponge after carbonization (B@ZnO/SG series).

analyzed with fourier-transform infrared spectroscopy (FTIR, Nicolet iS5). The crystallinity of obtained samples was investigated by X-ray diffractometer (XRD, Rigaku smartlab) with Cu Ka source. Thermogravimetric analysis (TGA) was performed using a thermogravimetric analyzer (TGA N-1000, Scinco) at a heating rate of 10 °C min^{-1} in air. Zeta potential of the materials dispersed in aqueous solution was determined using Zetasizer Nano-ZS90 (Malvern Instruments). The specific surface areas of the samples were investigated by the Brunauer–Emmett–Teller (BET) method with a Tristar II 3020 Micromeritics instrument. An X-ray photoelectron spectroscopy (XPS) analysis was performed using a Thermo VG Scientific Sigma Probe spectrometer.

Fabrication of electrodes

The slurries containing different active materials (SG or B@ZnO/SG samples) were prepared by mixing active materials (80 wt%), vapor grown carbon fiber (15 wt.%, VGCF, Showa Denko K.K.) and polyvinylidene fluoride (5 wt%, PVDF, Sigma-Aldrich) in N-methyl-2-pyrrolidone (NMP, 99%, Sigma-Aldrich). The electrodes were prepared by coating the slurries on 1 cm × 1 cm nickel foams, followed by vacuum drying at 60 °C for 12 h.

Electrochemical measurement

The electrodes were analyzed by cyclic voltammetry at a potential range of −1 to 0 V, impedance spectroscopy in a frequency range from 10 mHz to 100 kHz with an amplitude of 10 mV, and galvanostatic charge/discharge analysis (Autolab, P/G-Stat 100). Half-cells tests were carried out in 1M Na_2SO_4 aqueous electrolyte with Ag/AgCl (3 M KCl, 0.196 V vs. SCE, Metrohm) reference electrode, and Pt (1 cm × 1 cm) counter electrode, and the gap between the reference electrode capillary and the working electrode was maintained at 1–2 mm.

Results and discussion

The hierarchically porous carbon/ZnO composite electrodes were prepared from natural resources and polymeric waste as illustrated in Fig. 1(a). First, thin ZnO was deposited on a macroporous sponge surface as a seed layer by RF sputtering and arrays of ZnO nanowires were grown from the ZnO sputtered sponge surfaces in the zinc precursor solution. To control the length of ZnO nanowires, the growth reaction was allowed for 1, 3, and 5 h. Secondly, the ZnO/sponge structure was decorated with bacteria (*E. coli*) by a simple dropping of bacteria suspension onto the ZnO/sponge. Finally, bacteria captured ZnO/sponge samples were carbonized at 700 °C for 2 h. Fig. 1(b) shows macro the porous structure of a pristine sponge and a ZnO/sponge samples. After the ZnO sputtering and the growth reactions, the sample became brighter than the bare sponge, and the color of sponge-based samples got bright as the growth time of ZnO increased due to the intrinsic color of the ZnO. The growth of ZnO nanostructures on macroporous sponge was confirmed by SEM analysis. The pristine sponge shows a smooth surface, while ZnO sputtered sponge surface exhibits plenty of gaps over the sponge as shown in Fig. 1(c) and (d). After the ZnO growth reaction, homogeneous arrays of ZnO nanowires were observed throughout the sponge surfaces. As the growth reaction time of ZnO increased, the length of ZnO nanowire increased from 1 μm to 3 μm, while diameter of ZnO nanowires were almost maintained as shown in Fig. 1(e)–(g). Also, representative image of bacteria captured ZnO/SG5 prior to carbonization process is shown in Figure S1(a) and Fig. 1(h) (bare and false colored SEM images, respectively). The grown ZnO structure has the optimized needle-like morphology to capture bacteria by piercing bacteria cells; it gives a mechanical robustness to the ZnO structure after the bacteria capture. In addition, the gap between ZnO nanorods allow the efficient electrolyte penetration into the inner part of the electrode. This dramatically enhances the electrochemical reactions and kinetics of supercapacitors [21–23]. After carbonization, bacteria were not observed due to the disintegration and permeation of bacteria into the backbone of the pyrolyed sponge and surfaces of ZnO, and thereby resulting in the hybrid structure of ZnO/sponge coated with bacteria during thermal process as shown in Figure S1(b).

To chemically analyze the prepared materials, FTIR analysis of carbonized SG, and B@ZnO/SG series was performed (Fig. 2(a)). The characteristic peaks of ZnO were observed in the range of 500 cm–700 cm^{-1} which corresponds to Zn—O vibrations, and the peak intensity increased with ZnO growth time, indicating increase in ZnO contents [24,25]. Also, broad absorption peak at around 1600 cm^{-1} was also observed due to the O—H stretching bond. Especially, bacteria captured samples showed characteristic peaks of bacteria including amide region from 1700 to 1500 cm^{-1}, mixed region of proteins, lipids, and carbohydrates from 1500 to 1200 cm^{-1}, polysaccharide region from 1200 to 900 cm^{-1}, and the fingerprint region from 900 to 700 cm^{-1} [26,27]. These results implied that ZnO nanorods on sponge effectively captured bacteria during the bacteria doping process. The peak of bacterial became obvious as the ZnO growth time increased, which is associated with effective capture of bacteria on the ZnO nanorod.

The XRD patterns of the carbonized sponge and B@ZnO/SG series were investigated in order to prove the successful growth of ZnO (Fig. 2(b)). The broad peaks centered at around 25° and 45° were observed in all samples which assign to the (002) and (001) planes of carbon structure originated from the carbonized sponge as previously reported [28]. ZnO peaks were also observed at 2θ = 31.8, 34.5, 36.3, 47.6, 56.6, 62.9, 68.0, and 69.2°, which can be assigned to the (100), (002), (101), (102), (110), (103), (112), and (201) planes, respectively. Throughout this result, it was confirmed that the designed samples were well prepared without impurities and the intensity of ZnO peaks was significantly changed as a function of ZnO growth time, which is well in accordance with the SEM and FTIR analysis results.

In order to determine the contents of ZnO in B@ZnO/SG composite, thermogravimetric (TGA) analysis of carbonized sponge, and B@ZnO/SG series was carried out as shown in Fig. 2(c). TGA analysis of pure ZnO showed negligible weight loss (2.5 wt.%) after increasing the temperature up to 800 °C, and the small weight loss was primarily due to the evaporation of water. In the case of carbonized sponge and B@ZnO/SG series, slight weight losses were observed at 100 °C due to the evaporation of water. However, significant decrease in weight was observed in the range from 400 to 600 °C, which is attributed to the combustion of carbon from carbonized sponge and bacteria [29]. The weight fraction of residues of B@ZnO/SG samples at 800 °C, which correspond to the ZnO contents, increased from 0.34 to 17.9% when ZnO growth time increased from 1 to 3 h.

Zeta-potential of the prepared materials also analyzed as shown in Fig. 2(d). Amorphous carbon originated from carbonized sponge was negatively charged due to the defects of carbon structure [30,31]. In the case of B@ZnO/SG, all samples showed negative zeta potentials, and the negative charge of B@ZnO/SG decreased with ZnO growth time due to the increase of ZnO which has a positive surface charge around 10 mV. Even though positively charged ZnO was introduced, strong negative charges of bacteria originated from phospholipids and lipopolysaccharides provided a net negative charge of B@ZnO/SG [32,33]. The presence of more positive charges in the structure of B@ZnO/SG sample significantly improved their capturing ability of bacteria, which can be caused by the strong electrostatic attraction between ZnO and bacteria.

The BET experiments give useful information on the physical properties of surface area relevant to the electrochemical properties in Fig. 2(e). It was observed that the carbonized sponge had porous structures, and thus showed high specific area ($241\ m^2\ g^{-1}$). After ZnO sputtering (ZnO/SG0), the surface area was drastically reduced to $74\ m^2\ g^{-1}$, and this is because of the blockage of porous structures of sponge by sputtered ZnO and bacteria. However, the surface area of B@ZnO/SG increased with ZnO growth time from 167 to $319\ m^2\ g^{-1}$ when the ZnO growth reaction time increased from 1 to 5 h. This results imply that pores were created between ZnO nanowires, and it resulted in the increase of surface area. Moreover, B@ZnOS5 showed a higher surface area than that of the carbonized sponge. Importantly, high surface area of carbon materials generally provides good electrochemical properties because the capacitive behavior is mostly depending on the formation of double layer across the electrode/electrolyte interface [15,34–37].

To analyze the chemical composition of the carbonized sponge and B@ZnO/SG samples, the XPS analysis was performed, and XPS spectra were obtained in the range 0–1100 eV as shown in Fig. 2(f). In the case of the carbonized sponge, only C, N, and O peaks were observed. On the other hand, the carbonized B@ZnO/SG samples showed additional Zn peaks, and intensity of the ZnO peaks increased with ZnO growth time.

To further analyze the nitrogen species in the carbonized B@ZnO/SG samples, XPS data in the binding energy range from 390 to 407 eV were deliberately investigated as shown in Fig. 3. Three species of N-containing groups including pyridinic-N, pyrrolic-N and quaternary N could be verified by at 398.1, 399.4 and 401.1 eV, respectively (Fig. 3d) [38–40]. When the sponge was carbonized, pyridinic-N was mostly generated while contents of pyrrolic-N, and quaternary-N were increased as introducing bacteria that containing nitrogen source. Based on the results, bacteria were successfully incorporated into the ZnO/SG sampleswith providing nitrogen species. It implies that the needle-like morphology of ZnO was firstly interacted with surface of bacteria by morphological effect (needle-like structure) and electric charge interaction, then permeated the structure of carbon sources during the carbonization process. Pyridinic-N was most abundant at higher ZnO growth time because pyridinic-N was usually regarding to be more stable than other nitrogen species, indicating that B@ZnO/SG5 were more captured than other samples [41,42]. Finally, the results prove that carbonization process after capturing bacterial can allow the carbon skeleton to be doped with nitrogen species. It is well known that electrochemically active nitrogen atoms can easily control the delocalization of structures, resulting in plentiful accommodation of electrolyte ions on the electrode surface. In detail, pyridinic N and pyrrolic N play key roles in enhancing the specific capacitance of N-doped materials owing to their pseudocapacitive contribution [43–45].

In order to demonstrate the electrochemical behavior of sponge-based electrodes, cyclic voltammogram was investigated in a three-electrode system with 1 M Na_2SO_4 electrolyte in Fig. 4(a) and Figure S2. All the curves obtained from the sponge-based electrodes exhibited the distorted rectangular shape during charge/discharge processes, showing their combined capacitance from double layer capacitance and pseudo-capacitance due to the nitrogen species. The galvanostatic charge/discharge curves of the sponge-based electrodes at a current density of $0.2\ A\ g^{-1}$ exhibited the quasi-linear shape, indicating both EDLC and pseudocapacitive performance (Fig. 4(b) and Figure S3).

Figure S3 showed that the voltage curve profile between −1 and 0 V depending on the different current densities. Two distinct regions appeared during charging in voltage curves, one for which the voltage rapidly changes in the −1 to −0.5 V range, followed by a second region in which the voltage changes more gently between −0.5 and 0 V. In case of 3D structure, the surface of electrode (ZnO or ZnO/bacteria) was firstly reacted with the electrolyte ions. At this time, ZnO had the pseudocapacitive behavior, resulting in fast charging reaction. In the next step, the capacitive behavior of sponge was mostly dependent on the formation of double layer across the electrode/electrolyte interface. In discharging steps, the slope was dramatically changed at the high current density while the slope was slightly changed at low current density due to active electron transfer [46–48]. The specific capacitance of sponge-based electrodes calculated from galvanostatic charge/discharge curves at the $0.2\ A\ g^{-1}$ current density. The specific capacitance of

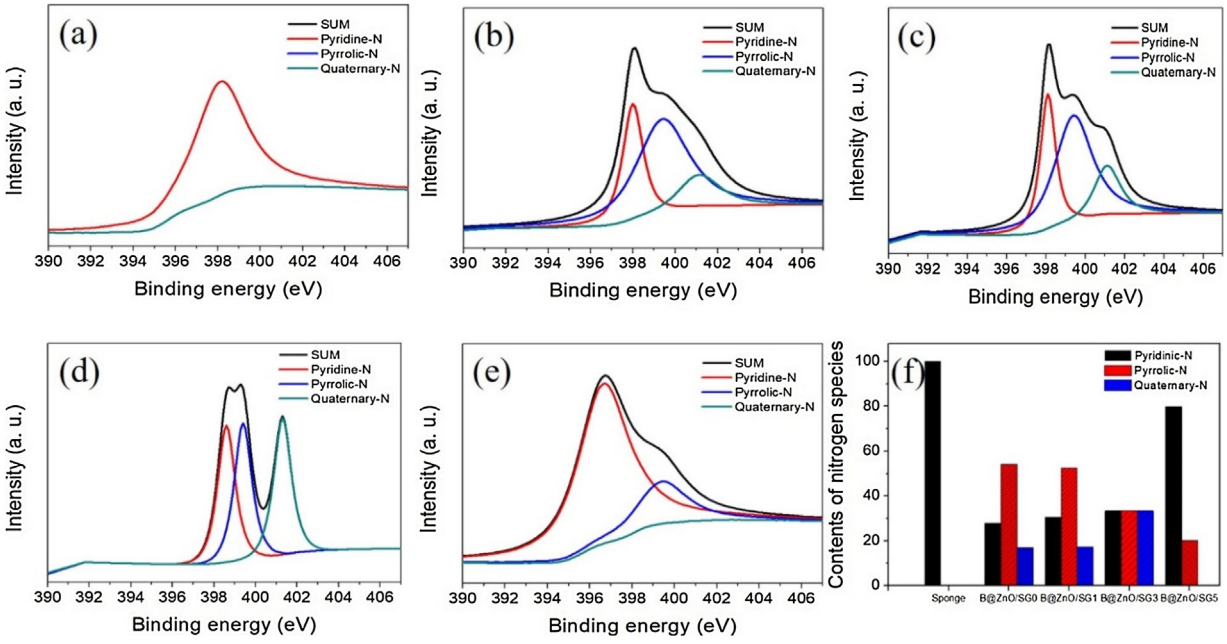

Fig. 3. XPS survey of (a) sponge, (b) B@ZnO/SG0, (c) B@ZnO/SG1, (d) B@ZnO/SG3, (e) B@ZnO/SG5, and (f) contents of nitrogen species with sponge, and bacteria captured ZnO on sponge with ZnO growth time.

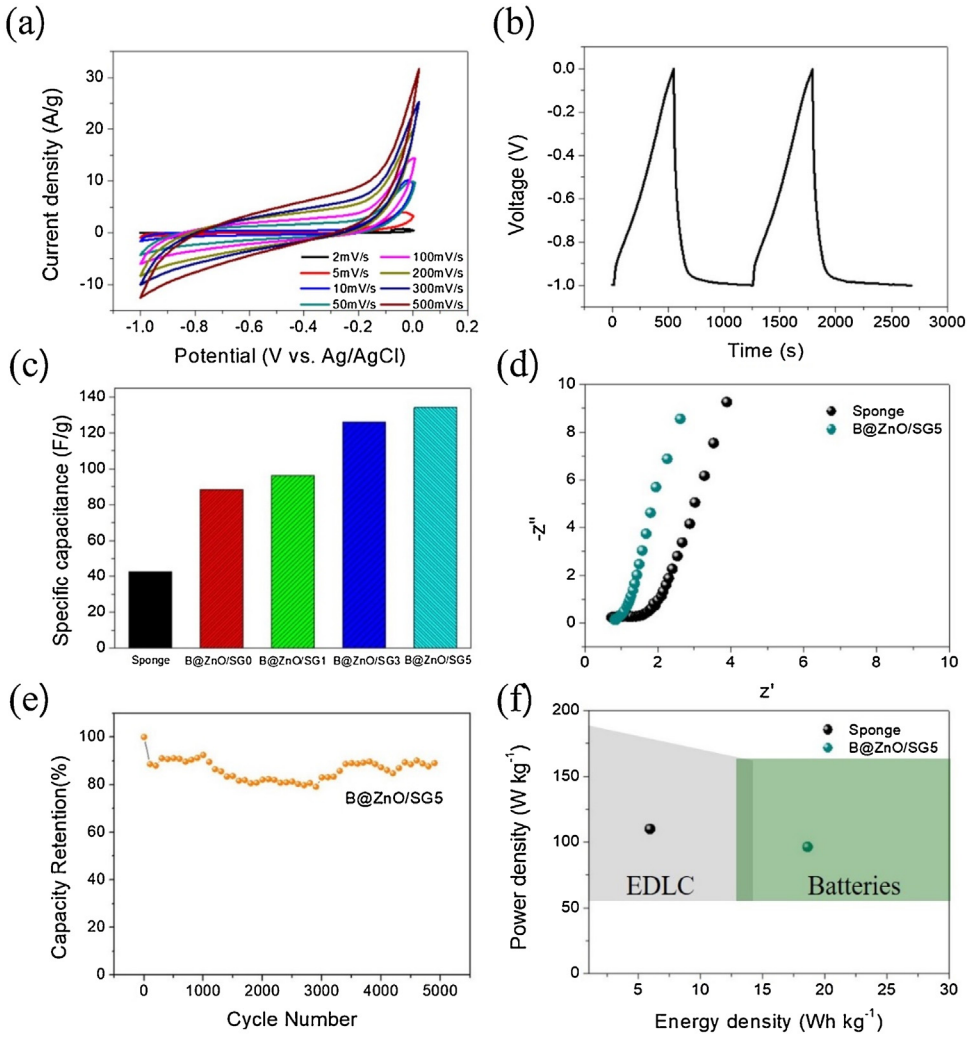

Fig. 4. Electrochemical evaluations of bacteria captured ZnO/SG electrodes: (a) cyclic voltammograms of B@ZnO/SG5 with various scan rates, (b) galvanostatic charge/discharge curve of B@ZnO/SG5 at 0.2 A/g, (c) specific capacitance, (d) Nyquist plots of sponge and B@ZnO/SG5, (e) cycling performance of B@ZnO/SG5, and (f) Ragone plot of sponge and B@ZnO/SG5.

the carbonized sponge was only 42 F/g from Fig. 4(b). After the bacteria were introduced and pyrolyzed, the specific capacitance was improved compared to that obtained from the pristine sponge. Also, the specific capacitance enhanced as growth time of ZnO was increased. It can be assumed that growth time of ZnO was relevant to bacteria capturing efficiency. ZnO nanowires with high aspect ratio can easily capture bacteria, which provide more abundant carbon and nitrogen sources as mentioned above. The B@ZnO/SG5 exhibited the most superior electrochemical performance, and the specific capacitance was 144 F g^{-1} at 0.2 A g^{-1} current density. The specific area and content of heteroatoms of which were the highest among the samples, indicating that there was a synergistic effect of ZnO and heteroatoms of bacteria. When the bacteria were directly loaded and carbonized on the bare sponge without ZnO (B@SG), the specific capacitance also increased to 64 F g^{-1} (Figure S3). However, the specific capacitance of B@ZnO/SG5 were drastically increased than that of B@SG, indicating that ZnO were also significant role in the composites by increasing surface area and intrinsic pseudocapacitance and interaction of bacteria, resulting improve specific capacitance.

Fig. 4(d) displayed Nyquist plots of B@ZnO/SG5 in a frequency range from 100 kHz to 10 mHz. The slope of the curve with low frequency region means the Warburg resistance, which is associated with the electrolyte and proton diff ;usion into the porous electrode. B@ZnO/SG5 exhibited lower diff ;usion resistance, indicating low charge-transfer resistance and high electrolyte accessibility, which could be explained by their surface area and nitrogen species [49]. In addition, the semicircle explained the charge-transfer process between electrode and electrolyte interface. The B@ZnO/SG5 with high surface area can cause lower the charge transfer resistance than the pristine sponge in Fig. 4(d). The cycle retention of B@ZnO/SG5 was investigated in order to assess the long-term cycle stability of the B@ZnO/SG5. After the 5000 charge–discharge cycle test, the B@ZnO/SG5 retained 89% of the initial specific capacitance, indicating outstanding cycling stability (Fig. 4(e)). The Ragone plot of the supercapacitor electrode showed that the highest energy density of 18 W h kg^{-1} can be reached at a power density of 96 W kg^{-1}, respectively in Fig. 4(f). This result reveals that the bacteria captured ZnO on sponge electrode demonstrated a superior electrode material.

Conclusions

We demonstrated a upcycle and renewable process for the fabrication of hierarchical carbon/ZnO composite electrodes for supercapacitors. Carbonization of polymeric sponge waste provided macroporous carbon skeleton. Carbonization of polymeric sponge waste provided macroporous carbon skeleton.

Hierarchically grown ZnO nanowires on a sponge surface provided not only a pseudocapacitive property but also an ability to capture bacteria cells which enable doping of carbon skeleton with electrochemically beneficial various nitrogen species. The resulting electrodes exhibited high surface areas due to hierarchical morphologies and high contents of nitrogen species originated from carbonized bacteria. The proposed sustainable chemistry utilizing multiple renewable resources to acquire required physicochemical properties will open new opportunities to prepare more functional materials in a more sustainable way. Also, it can be extended to other metal oxide compounds (e.g. nickel oxide, manganese oxide, cobalt oxide and etc.) and carbonaceous materials (e.g. activated carbon, graphite, carbon nanotube and etc.).

Acknowledgements

This research did not receive any specific grant from funding agencies in the public, commercial, or not-for-profit sectors.

Appendix A. Supplementary data

Supplementary material related to this article can be found, in the online version, at doi:https://doi.org/10.1016/j.jiec.2019.06.010.

References

[1] D. Larcher, J.-M. Tarascon, Nat. Chem. 7 (1) (2015) 19.
[2] Y. Zhu, C. Romain, C.K. Williams, Nature 540 (7633) (2016) 354.
[3] M. Zhou, F. Pu, Z. Wang, S. Guan, Carbon 68 (2014) 185.
[4] E. Fiset, T.E. Rufford, M. Seredych, T.J. Bandosz, D. Hulicova-Jurcakova, Carbon 81 (2015) 239.
[5] Z.J. Zhang, C. Dong, X.Y. Ding, Y.K. Xia, J. Alloys. Compd. 636 (2015) 275.
[6] G. Ma, D. Guo, K. Sun, H. Peng, Q. Yang, X. Zhou, X. Zhao, Z. Lei, RSC Adv. 5 (79) (2015) 64704.
[7] A. Elmouwahidi, E. Bailón-García, A.F. Pérez-Cadenas, F.J. Maldonado-Hódar, F. Carrasco-Marín, Electrochim. Acta 229 (2017) 219.
[8] X. Sun, P. Cheng, H. Wang, H. Xu, L. Dang, Z. Liu, Z. Lei, Carbon 92 (2015) 1.
[9] W. Yang, Q. Dong, S. Liu, H. Xie, L. Liu, J. Li, Procedia Environ. Sci. 16 (2012) 167.
[10] T.J. Beveridge, J. Bacteriol. 181 (16) (1999) 4725.
[11] D.-J. Scheffers, M.G. Pinho, Microbiol. Mol. Biol. Rev. 69 (4) (2005) 585.
[12] V. Augustyn, P. Simon, B. Dunn, Energy Environm. Sci. 7 (5) (2014) 1597.
[13] R.R. Salunkhe, J. Tang, Y. Kamachi, T. Nakato, J.H. Kim, Y. Yamauchi, ACS Nano 9 (6) (2015) 6288.
[14] R. Ramachandran, W. Xuan, C. Zhao, X. Leng, D. Sun, D. Luo, F. Wang, RSC Adv. 8 (7) (2018) 3462.
[15] H. Yong, H. Park, J. Jung, C. Jung, J. Ind. Eng. Chem. 76 (2019) 429.
[16] A. Yadav, A. Lokhande, J. Kim, C. Lokhande, J. Ind. Eng. Chem. 56 (2017) 90.
[17] F. Atalay, D. Asma, H. Kaya, E. Ozbey, Mater. Sci. Semicond. Process. 38 (2015) 314.
[18] H.-W. Shim, Y.-H. Jin, S.-D. Seo, S.-H. Lee, D.-W. Kim, ACS Nano 5 (1) (2010) 443.
[19] Y. Guo, B. Chang, T. Wen, C. Zhao, H. Yin, Y. Zhou, Y. Wang, B. Yang, S. Zhang, RSC Adv. 6 (23) (2016) 19394.
[20] M.A. Lim, D.H. Kim, C.-O. Park, Y.W. Lee, S.W. Han, Z. Li, R.S. Williams, I. Park, ACS Nano 6 (1) (2011) 598.
[21] T. Wang, D. Song, H. Zhao, J. Chen, C. Zhao, L. Chen, W. Chen, J. Zhou, E. Xie, J. Power Sources 274 (2015) 709.
[22] Z. Li, J. Han, L. Fan, M. Wang, S. Tao, R. Guo, Chem. Commun. 51 (15) (2015) 3053.
[23] D. Qi, Y. Liu, Z. Liu, L. Zhang, X. Chen, Adv. Mater. 29 (5) (2017)1602802.
[24] W. Hu, Y. Liu, T. Chen, Y. Liu, C.M. Li, Adv. Mater. 27 (1) (2015) 181.
[25] W. Hu, Y. Liu, Z. Zhu, H. Yang, C.M. Li, ACS Appl. Mater. Interfaces 2 (6) (2010) 1569.
[26] M.G. Kiran, K. Pakshirajan, G. Das, J. Hazard. Mater. 324 (2017) 62.
[27] C. Rubio, C. Ott, C. Amiel, I. Dupont-Moral, J. Travert, L. Mariey, J. Microbiol. Methods 64 (3) (2006) 287.
[28] M.V. Morales, E. Asedegbega-Nieto, A. Iglesias-Juez, I. Rodríguez-Ramos, A. Guerrero-Ruiz, ChemSusChem 8 (13) (2015) 2223.
[29] U. Suryavanshi, T. Iijima, A. Hayashi, Y. Hayashi, M. Tanemura, Chem. Eng. J. 179 (2012) 388.
[30] D. Wang, K. Wang, H. Wu, Y. Luo, L. Sun, Y. Zhao, J. Wang, L. Jia, K. Jiang, Q. Li, Carbon 132 (2018) 370.
[31] S. Gómez, N.M. Rendtorff, E.F. Aglietti, Y. Sakka, G. Suarez, Chem. Phys. Lett. 689 (2017) 135.
[32] B. Gottenbos, D.W. Grijpma, H.C. van der Mei, J. Feijen, H.J. Busscher, J. Antimicrob. Chemother. 48 (1) (2001) 7.
[33] S. Halder, K.K. Yadav, R. Sarkar, S. Mukherjee, P. Saha, S. Haldar, S. Karmakar, T. Sen, SpringerPlus 4 (1) (2015) 672.
[34] K.-J. Huang, L. Wang, J.-Z. Zhang, K. Xing, J. Electroanal. Chem. 752 (2015) 33.
[35] J.L. Qi, X. Wang, J.H. Lin, F. Zhang, J.C. Feng, W.-D. Fei, J. Mater. Chem. A 3 (23) (2015) 12396.
[36] Y. Tao, L. Ruiyi, Y. Tingting, L. Zaijun, Electrochim. Acta 152 (2015) 530.
[37] R. Farzana, R. Rajarao, B.R. Bhat, V. Sahajwalla, J. Ind. Eng. Chem. 65 (2018) 387.
[38] L. Lai, J.R. Potts, D. Zhan, L. Wang, C.K. Poh, C. Tang, H. Gong, Z. Shen, J. Lin, R.S. Ruoff, Energy Environ. Sci. 5 (7) (2012) 7936.
[39] Z. Zhang, L. Wang, Y. Li, Y. Wang, J. Zhang, G. Guan, Z. Pan, G. Zheng, H. Peng, Adv. Energy Mater. 7 (5) (2017)1601814.
[40] J. Wang, R. Huang, Y. Zhang, J. Diao, J. Zhang, H. Liu, D. Su, Carbon 111 (2017) 519.
[41] M. Sevilla, P. Valle-Vigón, A.B. Fuertes, Adv. Funct. Mater. 21 (14) (2011) 2781.
[42] K. Huang, S.-H. Chai, R.T. Mayes, G.M. Veith, K.L. Browning, M.A. Sakwa-Novak, M.E. Potter, C.W. Jones, Y.-T. Wu, S. Dai, Chem. Commun. 51 (97) (2015) 17261.
[43] H.M. Jeong, J.W. Lee, W.H. Shin, Y.J. Choi, H.J. Shin, J.K. Kang, J.W. Choi, Nano Lett. 11 (6) (2011) 2472.
[44] S. Li, C. Yu, J. Yang, C. Zhao, X. Fan, H. Huang, X. Han, J. Wang, X. He, J. Qiu, ChemElectroChem 4 (2) (2017) 369.
[45] K. Kan, L. Wang, P. Yu, B. Jiang, K. Shi, H. Fu, Nanoscale 8 (19) (2016) 10166.
[46] F.C. Walsh, L.F. Arenas, C. Ponce de León, J. Chem. Technol. Biotechnol. 93 (11) (2018) 3073.
[47] G. Xiong, P. He, Z. Lyu, T. Chen, B. Huang, L. Chen, T.S. Fisher, Nat. Commun. 9 (1) (2018) 790.
[48] S.P. da Silva, P.R.C. da Silva, A. Urbano, J. Scarminio, Quím. Nova 39 (8) (2016) 901.
[49] K.-P. Wang, H. Teng, J. Electrochem. Soc. 154 (11) (2007)A993.